Contents lists available at ScienceDirect

Proceedings of the Combustion Institute

journal homepage: www.elsevier.com/locate/proci





THz rotational absorption spectroscopy of the hydroxyl radical at high temperatures using a quantum-cascade laser

Nicholas M. Kuenning ^{a,*}, Nicolas Q. Minesi ^{a,b}, Brett A. Honaker ^a, R. Mitchell Spearrin ^a

- ^a Department of Mechanical and Aerospace Engineering, University of California, Los Angeles (UCLA), Los Angeles, CA, 90095, USA
- b Université Paris-Saclay, CNRS, CentraleSupélec, Laboratoire EM2C, 91190, Gif-sur-Yvette, France

ARTICLE INFO

Keywords: Hydroxyl Shock tube kinetics Laser absorption THz Rotational spectroscopy

ABSTRACT

A THz-frequency quantum-cascade laser absorption sensing method was developed for quantitative, time-resolved pure rotational spectroscopy of the hydroxyl radical in combustion environments. A systematic wavelength selection process involving consideration of line strength, temperature sensitivity, and spectral interference resulted in the down-selection of a group of rotational OH transitions near 531 cm $^{-1}$ (15.9 THz). Spectrally-resolved measurements of multiple transitions were achieved using a pulsed quantum-cascade laser (QCL) at a measurement rate of 25 kHz with an integration time of approximately 5 μ s. A neighboring water line within the scanning range of the laser enables the water spectra to be measured and subtracted, removing the already minimal water interference near the target OH feature. The THz-range sensor was integrated on a high-enthalpy shock tube to validate the line strengths of the selected OH transitions at or near equilibrium in shock-initiated oxidation of argon-diluted ethylene and oxygen mixtures over a range at temperatures between 1500–3500 K. Quantitative species time histories were also measured during chemical non-equilibrium of ethylene and methanol oxidation to demonstrate the capability to resolve transient formation and destruction OH during combustion. A detection limit of approximately 0.5 ppm-meter was demonstrated. To the authors' knowledge, this work represents the first laser absorption sensing of the pure rotational spectra of OH at combustion conditions, exhibiting high potential for numerous applications.

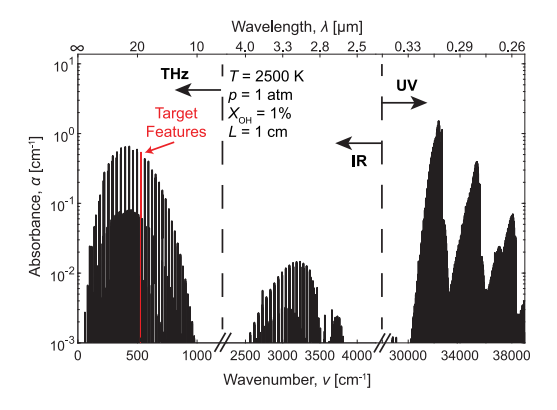
1. Introduction

The hydroxyl radical (OH) is a ubiquitous and critically important intermediate in the combustion of all hydrogen-containing fuels. Hydroxyl participates in the key chain-branching and propagation reactions that drive ignition and heat release. As a reactive intermediate, OH indicates both the onset and completion of combustion. Accordingly, in situ detection of the hydroxyl radical is of significant interest and value in experimental combustion studies. For reaction kinetics, OH emission or chemiluminescence serves as a primary indicator of ignition delay time [1,2]. In reacting fluid dynamics studies, laser-induced fluorescence of OH provides an indication of flame boundaries, while OH chemiluminescence imaging is a common approach to approximate the spatial distribution of heat release [3]. In the aforementioned optical diagnostic techniques, OH detection can be highly species-specific, but is usually not a quantitative metric for molecular abundance without extensive calibration.

Laser absorption spectroscopy (LAS) provides a means for calibration-free, quantitative and in-situ measurement of species concentration. Several LAS methods have been developed and employed for OH detection, with most work involving rovibronic transitions in the ultraviolet (UV) and associated light sources. The strongest UV transitions occur near 310 nm, leading many studies to target OH absorption with a variety of light sources such as pumped dyelasers and Ti:Sapphire lasers [4,5]. Despite the strong rovibronic OH transitions in the UV, the available light sources and associated optical configurations are large, costly, and lack fast tunability at combustion timescales, limiting more widespread deployment on combustion systems. By contrast, room-temperature semiconductor lasers in the near- to far-infrared offer access to the vibrational bands of various molecules with rapid injection-current tunability along with portability at modest cost, enabling broader applicability and ease-of-use relative to UV sources. However, the rovibrational spectra of OH in the nearto mid-infrared is difficult to probe in high-temperature combustion environments due to relative weakness in band intensity and spectral interference by stronger water and hydrocarbon absorption bands. A few attempts for IR-LAS in the near-IR (wavelength-modulation spectroscopy) and mid-IR (Faraday rotation) highlight the relatively weak rovibrational lines that are often obscured by interfering species,

E-mail address: kuenningn@g.ucla.edu (N.M. Kuenning).

^{*} Corresponding author.



 $Fig. \ 1. \ Hydroxyl \ radical \ absorbance \ simulations \ from \ HITEMP \ [11] \ data \ plotted \ across \ the \ relevant \ spectral \ ranges \ for \ combustion \ sensing.$

primarily $\rm H_2O$, creating challenges with regards to detection limits and species-specificity [6–8].

The THz spectral range provides potential for pure rotational spectroscopy and offers enhanced molecular detection capability for select species with strong rotational dipoles, such as the hydroxyl radical. As illustrated in Fig. 1, the rotational spectrum of OH is approximately 50 times stronger than its fundamental vibrational band in the infrared, while being of comparable strength to the rovibronic bands commonly targeted in the UV. The THz spectral range is largely free of interference from many common combustion species with rotational symmetry such as carbon dioxide, methane, and ethylene. Water vapor has a more comparable absorption intensity to the hydroxyl radical and requires careful wavelength selection to avoid interference. Recent advances in semiconductor light sources in the THz spectral range (1-30 THz), specifically quantum-cascade lasers (QCLs) [9,10], have made the rotational absorption spectra of OH and other important molecules accessible. Unlike the UV sources used to detect OH, quantum-cascade lasers provide a compact size and rapid tunability, characteristics of diodes and other semiconductor sources typical of the infrared.

This paper describes the development and first application of a THz quantum-cascade laser absorption sensor for quantitative, timeresolved pure rotational spectroscopy of the hydroxyl radical in combustion environments. In the following sections, the wavelength selection strategy and spectroscopic methods are detailed, along with the experimental optical setup on a high-enthalpy shock tube facility. Experimental results are presented based on spectrally-resolved measurements of OH using a pulsed QCL near 531 cm⁻¹ (15.9 THz) at well-known conditions of OH formation in order to validate the approach. Time-resolved measurements of OH formation during ethylene and methanol oxidation are also presented to demonstrate the sensor's time resolution. Detection limits are analyzed along with other limitations of the current THz-frequency optical configuration. To the authors' knowledge, this work represents the first high-temperature OH measurements in the pure rotational domain, demonstrating high potential for combustion sensing applications.

2. Methods

2.1. Wavelength selection

The pure rotational absorption spectrum of hydroxyl at 1500 K is shown in Fig. 2, highlighting the strong line intensities and broad THz spectral range spanned at high temperatures. Due to the relatively large rotational constant of OH ($B_e=18.9~{\rm cm}^{-1}$) in its ground electronic state, the rotational spectrum extends into the far-infrared domain at somewhat low rotational quantum numbers. The $X^2\Pi$ ground electronic state is a spin-split doublet, yielding multiple energy states for each rotational quanta, which are split again by Λ -doubling, where the

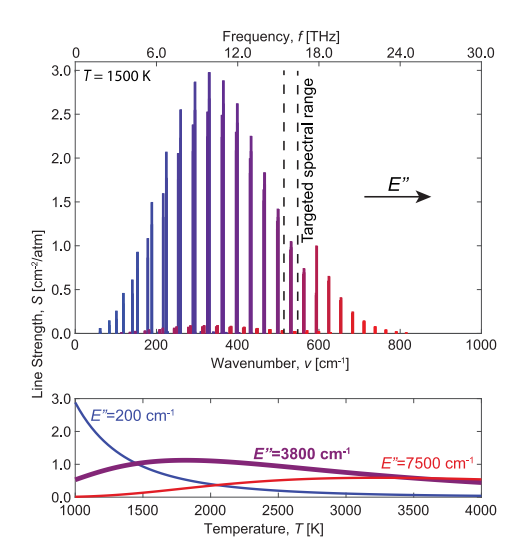


Fig. 2. (Top) Line strengths of rotational hydroxyl radical transitions from HITEMP [11] across the THz spectral range. (Bottom) Sample line strengths as a function of temperature at characteristic lower state energies. The lower state energy of the target transition is shown in bold.

internuclear electronic orbital angular momentum quantum number $\Lambda=1$ [12]. Each observed absorption feature, or apparent line, is the sum of two transitions that result from the proton hyperfine splitting, $<10^{-7}$ cm⁻¹ apart in wavenumber and $<10^{-6}$ cm⁻¹ apart in lower state energy. The spectroscopic approach employed here involves rapid tuning in wavelength to spectrally resolve individual lines, or sums of lines, to recover absorbance areas per Eq. (1):

$$\sum A_j = \int \alpha(\nu)d\nu = \sum S_j(T)X_{\text{abs}}PL \tag{1}$$

which relates the integrated absorbance areas A [cm $^{-1}$] of individual absorption transitions j to the mole fraction of the absorbing species X_{abs} , pressure p [atm], path length L [cm] and the temperature dependent line strength S(T) via the Beer–Lambert Law. Wavelength or line selection for narrowband semiconductor sources, which can tune over a few wavenumbers, is driven by relative line strength, temperature sensitivity (or insensitivity), and spectral isolation from other combustion species at high-temperature conditions.

Absorption simulations suggest that the magnitude of line strengths for many transitions within the pure rotational spectrum of OH (5 < J'' < 15) will enable single-ppm detection limits at conditions relevant to combustion experiments (T = 1500 K, L = 10 cm), providing a number of options for line selection. In addition to the magnitude of the line strength, it is desirable to select transitions with a lower-state energy that creates a weak dependence of line strength on temperature across the range of target temperatures, thus reducing uncertainty in species detection in applications with uncertain temperatures. In the pure rotational domain, lines at increasing frequency correspond to increasing lower-state energy E''. The relative temperature dependence of the absorption line strengths is primarily a function of the population fraction in the lower-energy state. Select lines labeled by their lower-state energy values are plotted in the bottom plot of Fig. 2. Higher-rotational-energy states become increasingly populated with increasing temperature, while the lower-energy states become depleted in accordance with the Boltzmann distribution. Individual lines with E'' \gtrsim 500 cm⁻¹ exhibit an increase in intensity with increasing temperature above 300 K, and subsequent peak and decline with further temperature increase. This work targets combustion environments, with a specific interest in the temperature range of 1000-3000 K. Accordingly, OH rotational lines with lower state energies in the range of 3500-4500 cm⁻¹ exhibit an insensitivity to temperature within the targeted temperature range, ($dS/dT \approx 0$ near 1500–2500 K), suggesting

Table 1Spectroscopic parameters of the target OH rotational transitions [11].

(cm^{-1})	$S_0(296 \text{ K})$ (cm ⁻² /atm)	$E_{ m low}$ (cm $^{-1}$)	Ω	J''	F''	par
529.6748	1.026	3842	1/2	13.5	14	f
529.6749	0.958	3842	1/2	13.5	13	f
530.5418	0.957	3847	1/2	13.5	13	e
530.5419	1.025	3847	1/2	13.5	14	e
531.0700	1.126	3811	3/2	14.5	15	e
531.0700	1.055	3811	3/2	14.5	14	e
532.1397	1.122	3819	3/2	14.5	15	f
532.1397	1.052	3819	3/2	14.5	14	f

that lines towards the higher end ($J'' \sim 15$) of the aforementioned target range are favorable.

Spectral interference was the last critical factor considered in the wavelength selection for pure rotational OH sensing. Notably, most common hydrocarbon combustion products and intermediates, including CO2, CO, H2, CH4, and C2H4, either lack a permanent dipole due to molecular symmetry or have a very weak one in rotation (CO pure rotational spectra is more than three orders of magnitude weaker than OH). Additionally, larger hydrocarbons with rotational asymmetry have much smaller rotational constants, and thus their pure rotational spectra are concentrated at much lower frequencies. The main exception is water vapor (H2O), which has similar rotational polarity to OH, and is a major combustion product. Several rotational line groupings of OH were closely examined for water interference in the 500-600 cm⁻¹ range (15-18 THz), representing a range of rotational quanta between 12-16. Figure 3 shows the simulated absorbance and line strengths of the targeted features. As depicted, water absorbance features are approximately 10x weaker than the hydroxyl radical (note the concentration of H₂O in Fig. 3 is 10x that of OH). It is common for water to have a significantly higher concentration than the hydroxyl radical at many combustion conditions, making the interference non-negligible; however, an advantage of scanning the laser in wavenumber means the water interference can be measured and subtracted. A fitting procedure accounting for water interference is detailed in Section 2.3. In summary, the transitions near 531 cm⁻¹ (15.9 THz) were selected because of their line strength, temperature insensitivity at $E'' = 3800 \text{ cm}^{-1}$, and minimal water interference.

Table 1 summarizes the key spectroscopic parameters of the lines plotted in Fig. 3. The quantum number defining the total angular momentum of the lower state, excluding nuclear spin, is represented by J'' and the quantum number defining total angular momentum, including nuclear spin, is labeled F''. Both J'' within the spectral region have two transitions associated with them due to Λ -doubling, labeled by the rotationless parity 'e' or 'f' in Table 1. The inverted energy level progression of the OH transitions results in lower energy states for J''states with $\Omega = 3/2$ compared to their $\Omega = 1/2$ counterpart [13]. The quantum numbers Ω , J'', and F'', in combination with the rotationless parity, fully define each rotational state. The J'' = 13.5 rotational states have four additional transitions near $v = 499 \text{ cm}^{-1}$ ($\Omega = 3/2$) and the J'' = 14.5 transitions have four additional transitions near v = 562 cm⁻¹ ($\Omega = 1/2$), completing the set of eight transitions expected for each rotational state of OH in the ground state vibrational mode and $X^2\Pi$ electronic state.

2.2. Shock tube optical setup

The THz-range laser-absorption sensor was integrated with a shock tube facility, used to generate controlled high-temperature conditions relevant to combustion environments. Hydroxyl radicals (and other combustion species) were generated by shock heating mixtures of ethylene/oxygen and methanol/oxygen diluted in argon using the UCLA high-enthalpy shock tube facility, described in previous works [14]. Figure 4 shows a cross-section of the instrument configuration located

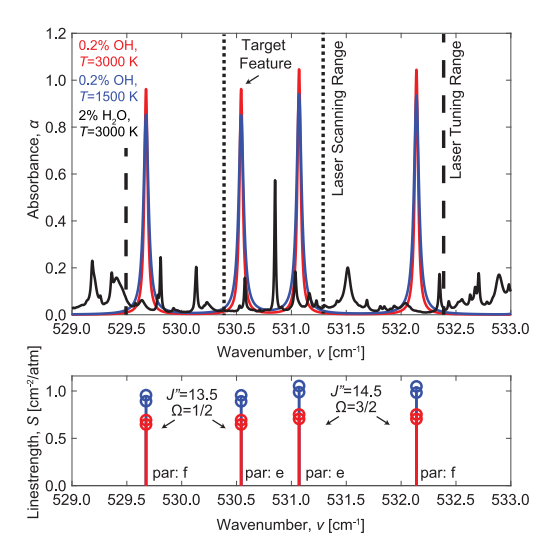


Fig. 3. (Top) Absorbance of the hydroxyl radical and water interference simulated with HITEMP [11] data over the spectral range accessible by the light source used in this study. Simulations were performed at 2 atm with the collisional broadening coefficients of air. (Bottom) Line strengths of potential target transitions with spectroscopic labeling.

2 cm from the shock tube end wall. A dynamic pressure transducer (Kistler 601B1) and optical windows are mounted flush to the inner surface of the tube, which has an internal diameter of 10.32 cm. Laser light at $5.0\,\mu m$ and $18.8\,\mu m$ was passed through sapphire and zincselenide windows respectively. The pressure time history of the incident and reflected shock wave was recorded through a charge amplifier (Kistler Type 5018A), and five piezoelectric sensors (Dynasen CA-1135) recorded the time of arrival of the incident shock wave, from which the incident shock velocity and reflected shock test conditions are determined using normal-shock relations [15]. Example raw voltage data from the detectors and pressure transducer, shown in the top of Fig. 4, were recorded at 1.25 GHz using a Tektronix MS044 acquisition module, triggered to record by the time-of-arrival sensors. Spectrallyresolved OH and CO absorption measurements, at 25 kHz and 100 kHz respectively, were performed in the shock tube for a reflected shock temperature (T₅) range of 1300-3500 K and a reflected shock pressure (P_5) range of 2–6 atm using scanned-wavelength techniques.

Hydroxyl-radical absorption measurements were performed at 18.8 µm (15.9 THz) with a room-temperature, tunable pulsed quantumcascade laser (QCL) provided by MirSense. The tuning range of the laser is between 529.5-532.4 cm⁻¹, in a single pulse the laser scans over 0.7 \mbox{cm}^{-1} when driven with a $10\,\mu s$ pulse at a 25% duty cycle, providing a measurement rate of 25 kHz. Injection-current pulses were generated by a Rigol-DG1032 function generator and passed through an Arroyo 6310-QCL controller before being delivered to the laser. These settings provide an output peak power of 10 mW with an average power >1 mW. Figure 3 shows both the laser tuning range and the wavenumber range covered by a single pulse. The laser intensity was collected on a liquid nitrogen-cooled Teledyne-Judson J15D22-M204-S250U-60 detector attached to a PA-102 preamplifier with a bandwidth of 1 MHz. Additionally, rovibrational transitions of carbon monoxide were targeted near 5.0 µm to obtain temperature, pressure, and CO mole fraction. CO measurements were made at 100 kHz with a distributed-feedback QCL and recorded on a photovoltaic detector. This carbon monoxide transition and its associated data processing has been extensively detailed in previous works and is omitted here for brevity [16].

Mixtures of ethylene (>99.999%)/oxygen (>99.999%) and methanol (>99.6%)/oxygen diluted in argon (>99.999%) were prepared manometrically in an agitated mixing tank before being routed to the shock tube test section through a gas-delivery manifold. Methanol

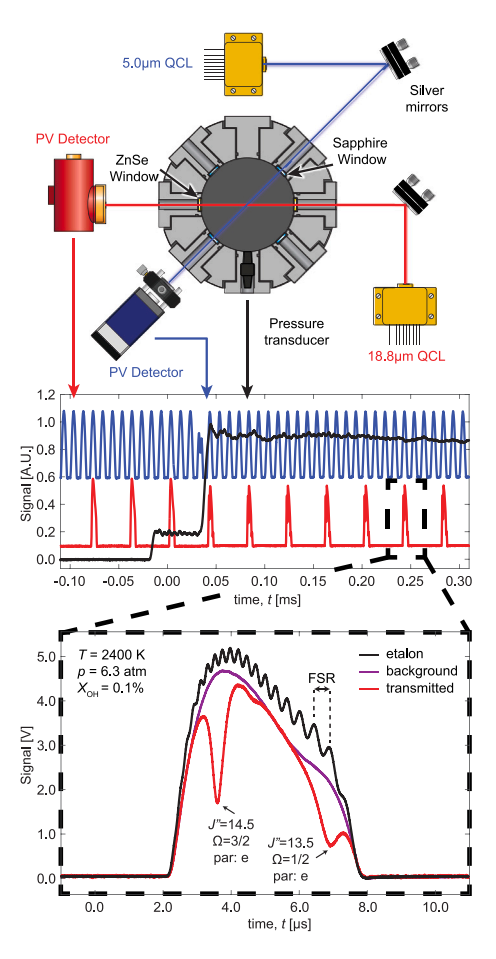


Fig. 4. (Top) Shock tube cross-section showing light sources and detectors. (Middle) Raw data traces during the pre-shock, incident shock, and reflected shock regions. (Bottom) Sample single measurement scan showing the scan alignment with the background and etalon scans.

has a vapor pressure near 100 Torr, raising concerns about the concentration changing due to adsorption to the walls of the mixing tank and shock tube. These losses were mitigated through a passivation procedure described in previous works [17]. Mixtures were left in the agitated mixing tank for a minimum of 30 min prior to filling the shock tube to ensure homogeneity.

2.3. Spectroscopic data processing

Raw intensities are converted to absorbance through the relation $\alpha(v) = -\ln{(I_t/I_0)}$. The transmitted signal I_t , consists of scans recorded past the arrival of the reflected shock and the background signal I_0 , is the average of all scans before the arrival of the incident shock. Arrival of the reflected shock is determined by observing the slight signal attenuation of the CO laser due to beam steering as is shown in the top plot of Fig. 4. A sample transmitted scan and the averaged background is shown in Fig. 4.

A mapping between the time domain and wavenumber domain is required to determine the absorbance as a function of wavenumber. This map is created before the test by aligning the laser perpendicularly through a 10.32-cm cavity bounded by two ZnSe windows and vacuumed to <10 mTorr. The resulting pattern of constructive and destructive interference contains peaks of known wavenumber spacing, or free spectral range (FSR), shown in Fig. 4. As the scan progresses in time, the laser wavenumber decreases. The higher density of peaks per unit of time in the initial portion of the scan represents the laser

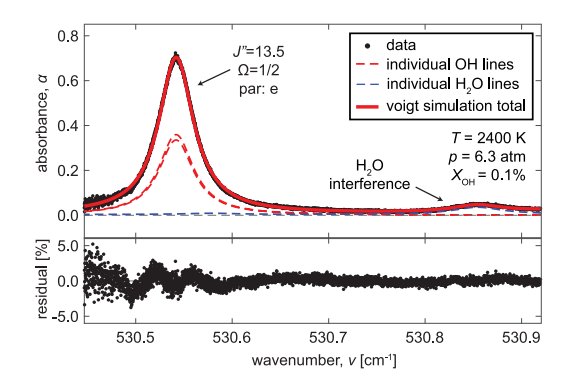


Fig. 5. (Top) Measured absorbance spectra during ethylene oxidation and resulting Voigt fit containing one OH feature and water interference. (Bottom) Residual between the measured absorbance spectra and Voigt fit. (For interpretation of the references to color in this figure legend, the reader is referred to the web version of this article.)

scanning faster in response to the sharp leading edge of the injectioncurrent pulse. Later in the scan, the peak density decreases while scanning over the J'' = 13.5 feature. The J'' = 13.5 feature was used for all measurements in this work because the J''=14.5 line is more instrument-broadened by detector bandwidth limitations. It should be noted that the instrument broadening has minimal effect on the absorbance area. Figure 5 shows the measured absorbance calculated from the transmitted and background scans plotted against wavenumber, transformed from the time domain. Areas are extracted from the measured absorbance spectra through a Voigt fitting routine. A Voigt line shape is specified by a Doppler width and collisional width. If the temperature is known then the Doppler width is fully defined and only the collisional width needs to be determined. Within the fitting routing, the area, collisional width, and spectral position of each OH feature were floated. Each feature consists of two closely spaced transitions with nearly the same center wavenumber and lower state energy, as shown in Table 1. The uncertainty introduced by summing these features, instead of fitting individual lines, is negligible. Additionally, the water spectrum is simulated using the HITEMP database, floating the mole fraction of water within the fit routine to subtract out water interference [11]. The water absorbance simulation is anchored in wavenumber to the most prominent line centered near 530.85 cm⁻¹. The resulting fit is shown as a solid red line in the top plot of Fig. 5 and the resulting residual is shown in the bottom plot. The simultaneous fit of the water spectra corrects for the minor interference at the OH lines and avoids biasing the OH measurement.

3. Results and discussion

3.1. Line strength validation

The HITEMP database does not list line strength uncertainties for the lines targeted in this study, necessitating validation of the reported reference line strengths [11]. Line strength calculations require an absorbance spectra measurement of a known hydroxyl radical concentration at a known temperature and pressure. After extracting the integrated area of the absorbance feature and using the known thermodynamic conditions, the line strength, or in this case the summed line strengths, is calculated via Eq. (1). Figure 6 visualizes the process used here for calculating the line strength at a given temperature. Stoichiometric mixtures of ethylene and oxygen, diluted in 99% argon, were shock heated to a desired temperature and pressure and the resulting absorbance spectra of CO and OH were measured. The CO absorbance measurements are converted to a CO mole fraction, temperature, and pressure as plotted in Fig. 6. OH absorbance measurements are Voigt fit to obtain the integrated absorbance areas following the procedure outlined in Section 2.3. Five established chemical kinetic mechanisms,

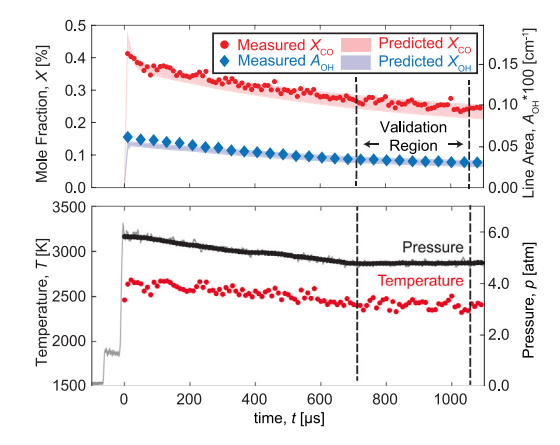


Fig. 6. (Top) Time evolution of OH integrated absorbance area and CO mole fraction compared to simulated mole fractions during an ethylene oxidation test. (Bottom) Time evolution of pressure transducer, optical pressure from CO, and temperature measurements.

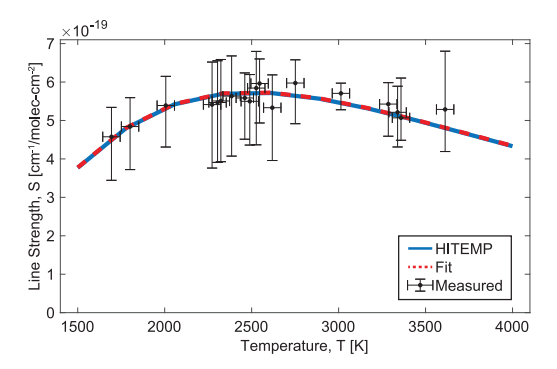


Fig. 7. Measured line strengths as a function of temperature, and their respective fit, compared to line strengths predicted by HITEMP [11].

ARAMCO [18], San Diego [19], USC II [20], FFCM [21], and LLNL [22] were used to simulate OH and CO mole fractions, fixing the temperature and pressure to the measured conditions. The range of species mole fraction predicted by these mechanisms is plotted as a solid area in the top plot of Fig. 6. Carbon monoxide species measurements serve as a useful metric of the agreement between the mechanisms and the measured concentrations over the test time. Minor disagreements between mechanisms and data may exist near the ignition event but it is expected that as the reaction approaches equilibrium, the mechanisms and the measurement will exhibit better agreement. Within the times labeled 'Validation Region' in Fig. 6, the measured CO concentration is within the range predicted by the kinetic mechanisms. Additionally, both the temperature and pressure trace are relatively flat compared to previous times. At these conditions, the averaged OH area, temperature, and pressure are used to calculate the line strength.

Line strengths measured over a range of conditions from 1700–3600 K and 2–6 atm are shown as black markers in Fig. 7. The function describing the temperature dependence of the line strength function can be simplified to a reference line strength, $S(T_0)$, multiplied by a temperature-dependent term that relies on accurate knowledge of the partition function and lower-state energy [13]. Floating the sum of reference line strengths in a least-squares fitting routine to all measured data yields a sum of reference line strengths that is within 1% of the HITEMP data. The measured value of linestrength here, which again is a sum of two lines, has an experimental uncertainty of $\pm 14\%$, reflected in the error bars shown in Fig. 7. The line strength is relatively flat over a range of temperatures between 1500–3500 K, meaning uncertainties in the temperature of an absorbing species have a relatively weak effect on the inferred mole fraction uncertainty. It

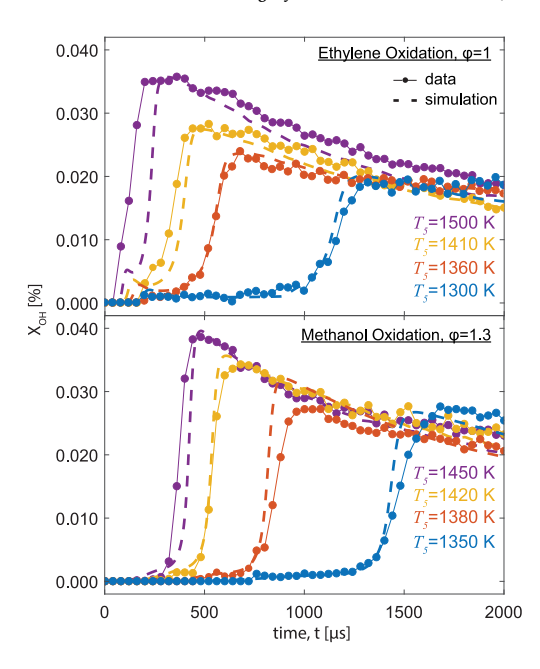


Fig. 8. Measured and simulated (San Diego Mechanism [19]) OH mole fraction in shock-heated mixtures of ethylene and oxygen in 99% argon (Top) and methanol and oxygen in 99% argon (Bottom). Region 5 pressures (p_5) between 3.1–3.3 atm were targeted for all tests.

should be noted that the line strength is a constant multiplied by a well-defined temperature-dependent Boltzmann distribution function for a given lower-state energy assignment, and the reference linestrength can be measured at any temperature [23]. Multiple measurements were performed at different temperatures to reduce uncertainty.

3.2. Time-resolved combustion sensing

Hydrocarbon oxidation tests were performed on mixtures of stoichiometric ethylene/oxygen and rich ($\phi = 1.33$) methanol/oxygen mixtures diluted in 99% argon to demonstrate time-resolved measurements of the transient formation and destruction of the hydroxyl radical. Experiments for each reactant combination were performed over a range of temperatures to highlight the capability of the OH sensor to resolve variations in temporal behavior resulting from the highly-temperature-dependent oxidation kinetics. The hydroxyl radical is a key intermediate present in both ethylene and methanol oxidation, indicating the onset of ignition in addition to the progression of the reaction. Figure 8 shows the quantitative time histories of OH mole fraction after the respective fuels were shock heated. Data for each test is collected at a measurement rate of 25 kHz, corresponding to the laser scan rate, and with a measurement integration time of approximately 5 μs, reflecting the portion of the laser scan period needed to resolve the target OH lines and H₂O correction line. Species time histories predicted by the San Diego mechanism [19], anchored to the temperature inferred from the CO spectra and the pressure recorded by the Kistler pressure transducer, are plotted for comparison in Fig. 8. The expected trends of shortening ignition delay with increasing temperature are clearly resolved, while the general convergence of OH mole fraction at longer timescales is also measured.

3.3. Detection limits and uncertainties

The detection limit of absorption measurements is mainly set by the noise of the detection system, resulting in a total absorbance noise of $\alpha_{\rm noise}=0.0025$. The uncertainty in the area is approximated by multiplying the absorbance noise by the line width. Applying this area

uncertainty calculation to a range of tests from this study provides a minimum detectable (SNR = 2) OH mole fraction of approximately 5 ppm at 1500 K. This detection limit value varies minimally with temperature due to the insensitivity of line strength to temperature, and is also relatively insensitive to pressure (up to at least about 8 bar) due to the linewidth being in the Lorentzian limit.

Uncertainty in line strength measurements is dominated by the uncertainties in the reference kinetic models and experimental temperature. The uncertainty of the temperature inferred by CO measurements was obtained by running a series of shocks on pure CO, diluted in 99% argon, over a range of temperatures between 2000-3500 K. Since CO does not undergo chemical reactions at these conditions, the calculated post-shock temperatures are accurate throughout the test and the comparison between the calculated post-shock temperatures and the measured temperature from CO was ±50 K, consistent with the spread in measured temperatures seen in Fig. 6. The horizontal error bars of Fig. 7 represent this ±50 K uncertainty. This temperature uncertainty is propagated, along with the uncertainty in the mechanisms, by simulating the OH mole fraction evolution predicted by the five mechanisms at the measured temperature ±50 K. The resulting maximum and minimum values are plotted as the vertical error bar bounds in Fig. 7. Individually, the uncertainties introduced from temperature and disagreements between mechanisms introduce ±10% error each, summing the error in quadrature results in a reference line strength uncertainty of ±14%.

The relatively low detection bandwidth, compared to the laser pulse frequency, puts measurements at risk of being biased by instrument broadening. Line shape distortion takes place when the laser scans over the full width half maximum at a rate that exceeds half the bandwidth. Sensing is currently limited to pressures >2 atm in order to mitigate attenuation from instrument broadening, below 2 atm the area attenuation from bandwidth limitations becomes >5%. These bounds were obtained by performing the fitting routine described in Section 2.3 on simulated spectra that were passed through a second-order digital low-pass filter with a 3 dB cutoff of 1 MHz, representing the detector pre-amplifier. The etalon measurement obtained in Fig. 4 was used to map the simulated spectral domain to the time domain. Fit results were compared to the known concentration of the simulation to quantify the uncertainty introduced by instrument broadening. Advancements could be made in future work by increasing the bandwidth of the detection system, currently limited by the 1 MHz bandwidth of the pre-amplifier of the PV-detector. Obtaining a pre-amplifier with a higher bandwidth would reduce instrument broadening and enable measurement rates above 100 kHz. The laser specifications allow pulses as narrow as 0.3 μs, enabling measurement rates up to 800 kHz with a satisfactory detection system.

4. Conclusion

This work demonstrated the ability of newly available light sources in the THz spectral range to perform time-resolved, quantitative measurements of the hydroxyl radical at combustion conditions. Pure rotational transitions of OH near $18.8\,\mu m$ (15.9 THz) were probed at 25 kHz using a quantum-cascade laser to resolve the species time evolution of OH behind shock-heated mixtures of ethylene/oxygen and methanol/oxygen diluted in argon. A spectral fitting routine was developed to measure and subtract the H2O spectra within the targeted region, correcting the minor effect of interfering species. The line strength value of the $J''=13.5,\ \Omega=1/2,$ e-parity feature in the HITEMP OH database was validated within ±14% uncertainty. Subsequently, the time-resolution capability of the sensor was demonstrated by performing measurements of OH formation and decay during the high-temperature oxidation of two fuels, ethylene and methanol. A detection limit of approximately 5 ppm at combustion temperatures was demonstrated for an optical path length of 10 cm. To the authors' knowledge, this work represents the first laser absorption sensing of the

pure rotational spectra of OH at combustion conditions. Importantly, the semiconductor laser used here for THz sensing is orders of magnitude smaller than UV lasers used for measuring rovibronic OH transitions, safer due to the long wavelength, and rapidly tunable offering quick alignment and robustness – correction of beam steering, thermal emission, laser drift, and unknown line broadening – in harsh environments enabled by the scanned-wavelength approach [23]. As such, this laser diagnostic method shows promise for future use in practical combustion devices, providing high-speed quantitative measurements of OH in a compact, robust, low-cost sensor package.

Novelty and significance statement

The novelty of this research is in being the first THz-range laser absorption spectroscopy study probing the pure rotational hydroxyl transitions in combustion environments. It is significant because this study establishes the feasibility of making quantitative hydroxyl radical measurements with a compact, rapidly-tunable semiconductor source, enabling future development of portable high-speed OH diagnostics systems for broad use in combustion studies.

CRediT authorship contribution statement

Nicholas M. Kuenning: Writing – review & editing, Writing – original draft, Visualization, Validation, Software, Methodology, Investigation, Formal analysis, Data curation. Nicolas Q. Minesi: Writing – review & editing, Supervision, Methodology, Conceptualization. Brett A. Honaker: Software, Methodology, Investigation. R. Mitchell Spearrin: Writing – review & editing, Writing – original draft, Supervision, Resources, Project administration, Methodology, Funding acquisition, Conceptualization.

Declaration of competing interest

The authors declare that they have no known competing financial interests or personal relationships that could have appeared to influence the work reported in this paper.

Acknowledgments

This work was supported by the U.S. National Science Foundation, CAREER Award No. 1752516, and by the Air Force Office of Scientific Research (AFOSR), USA DURIP award no. FA9550-21-1-0467 with Dr. Chiping Li as Program Officer. The authors thank Prof. Benjamin Williams for useful discussion regarding the laser and detection system. Additionally, the authors thank Eilam Morag for assistance and discussion surrounding the initial setup of the laser.

References

- [1] S. Saxena, M.S. Kahandawala, S.S. Sidhu, A shock tube study of ignition delay in the combustion of ethylene, Combust. Flame 158 (6) (2011) 1019–1031, Publisher: The Combustion Institute.
- [2] T. Kathrotia, M. Fikri, M. Bozkurt, M. Hartmann, U. Riedel, C. Schulz, Study of the H+O+M reaction forming OH*: Kinetics of OH* chemiluminescence in hydrogen combustion systems, Combust. Flame 157 (7) (2010) 1261–1273.
- [3] Y. Hardalupas, M. Orain, Local measurements of the time-dependent heat release rate and equivalence ratio using chemiluminescent emission from a flame, Combust. Flame 139 (3) (2004) 188–207.
- [4] R.K. Hanson, S. Salimian, G. Kychakoff, R.A. Booman, Shock-tube absorption measurements of OH using a remotely located dye laser, Appl. Opt. 22 (5) (1983) 641
- [5] S. Wang, R.K. Hanson, High-sensitivity 308.6-nm laser absorption diagnostic optimized for OH measurement in shock tube combustion studies, Appl. Phys. B 124 (3) (2018) 37.
- [6] T. Aizawa, Diode-laser wavelength-modulation absorption spectroscopy for quantitative in situ measurements of temperature and OH radical concentration in combustion gases, Appl. Opt. 40 (27) (2001) 4894.

- [7] T.R.S. Hayden, N. Malarich, D. Petrykowski, S.P. Nigam, J.D. Christopher, C. Lapointe, N.T. Wimer, P.E. Hamlington, G.B. Rieker, OH radical measurements in combustion environments using wavelength modulation spectroscopy and dual-frequency comb spectroscopy near 1491 nm, Appl. Phys. B 125 (12) (2019) 226
- [8] W. Zhao, G. Wysocki, W. Chen, W. Zhang, High sensitivity Faraday rotation spectrometer for hydroxyl radical detection at 2.8 μ m, Appl. Phys. B 109 (3) (2012) 511–519.
- [9] B.S. Williams, Terahertz quantum-cascade lasers, Nat. Photonics 1 (9) (2007) 517–525.
- [10] M. Carras, G. Maisons, J. Abautret, R. Teissier, F. Boulila, M. Brun, T. Shutz, M. Guais, Recent improvements of quantum cascade lasers for DIRCM at mirSense, in: R.J. Grasso, M. Eichhorn, G.D. Lewis (Eds.), Technologies for Optical Countermeasures XIX, SPIE, Amsterdam, Netherlands, 2023, p. 10.
- [11] L. Rothman, I. Gordon, R. Barber, H. Dothe, R. Gamache, A. Goldman, V. Perevalov, S. Tashkun, J. Tennyson, HITEMP, the high-temperature molecular spectroscopic database, J. Quant. Spectrosc. Radiat. Transfer 111 (15) (2010) 2139–2150.
- [12] G. Herzberg, Molecular Spectra and Molecular Structure II. Infrared and Raman Spectra of Polyatomic Molecules, D. Van Nostrand Company, Inc., Princeton, NJ, 1945.
- [13] R. Hanson, R. Spearrin, C. Goldenstein, Spectroscopy and Optical Diagnostics for Gases, Springer International Publishing, 2016.
- [14] F.A. Bendana, D.D. Lee, C. Wei, D.I. Pineda, R.M. Spearrin, Line mixing and broadening in the v(1→3) first overtone bandhead of carbon monoxide at high temperatures and high pressures, J. Quant. Spectrosc. Radiat. Transfer 239 (2019) 106636, Publisher: Elsevier Ltd.

- [15] J.D. Anderson, Modern Compressible Flow, McGraw-Hill, 2002.
- [16] A. Nair, D. Lee, D. Pineda, J. Kriesel, W. Hargus, J. Bennewitz, S. Danczyk, R. Spearrin, MHz laser absorption spectroscopy via diplexed RF modulation for pressure, temperature, and species in rotating detonation rocket flows, Appl. Phys. B 126 (8) (2020) 138.
- [17] N.M. Kuenning, I.C. Sanders, N.Q. Minesi, D.I. Pineda, R.M. Spearrin, High-temperature absorption cross-sections and interference-immune sensing method for formaldehyde near 3.6-μm, J. Quant. Spectrosc. Radiat. Transfer 309 (2023) 108690.
- [18] U. Burke, W.K. Metcalfe, S.M. Burke, K.A. Heufer, P. Dagaut, H.J. Curran, A detailed chemical kinetic modeling, ignition delay time and jet-stirred reactor study of methanol oxidation, Combust. Flame 165 (2016) 125–136.
- [19] H.J. Curran, Developing detailed chemical kinetic mechanisms for fuel combustion, Proc. Combust. Inst. 37 (1) (2019) 57–81.
- [20] H. Wang, X. You, A.V. Joshi, S.G. Davis, A. Laskin, F. Egolfopoulos, C.K. Law, et al., USC mech version II. High-temperature combustion reaction model of H2/CO/C1-C4 compounds, 2007.
- [21] G.P. Smith, Y. Tao, H. Wang, Foundational fuel chemistry model version 1.0 (FFCM-1), 2016.
- [22] N.M. Marinov, W.J. Pitz, C.K. Westbrook, A.M. Vincitore, M.J. Castaldi, S.M. Senkan, C.F. Melius, Aromatic and polycyclic aromatic hydrocarbon formation in a laminar premixed n-butane flame, Combust. Flame 114 (1–2) (1998) 192–213.
- [23] C. Goldenstein, R. Spearrin, J. Jeffries, R. Hanson, Infrared laser-absorption sensing for combustion gases, Prog. Energy Combust. Sci. 60 (2017) 132–176.